J|A|C|S
ARTICLES

Published on Web 12/15/2008

Ammonia Triborane: A New Synthesis, Structural Determinations, and Hydrolytic Hydrogen-Release Properties

Chang Won Yoon, Patrick J. Carroll, and Larry G. Sneddon*

Department of Chemistry, University of Pennsylvania, Philadelphia, Pennsylvania 19104-6323

Received October 17, 2008; E-mail: lsneddon@sas.upenn.edu

Abstract: Iodine oxidation of $B_3H_8^-$ in glyme solution to produce (glyme)B_3H_7, followed by displacement of the coordinated glyme by reaction with anhydrous ammonia provides a safe and convenient preparation of ammonia triborane, $NH_3B_3H_7$ (**1**). X-ray crystallographic determinations and DFT computational studies of both $NH_3B_3H_7$ and the $NH_3B_3H_7$·18-crown-6 adduct demonstrate that while computations predict a symmetric single bridging-hydrogen conformation, $NH_3B_3H_7$ has a highly asymmetric structure in the solid-state that results from intermolecular $N-H^+\cdots H^--B$ dihydrogen bonding interactions. Studies of its hydrolytic reactions have shown that upon the addition of acid or an appropriate transition metal catalyst, aqueous solutions of **1** rapidly release hydrogen, with 6.1 materials wt % H_2-release being achieved from a 22.7 wt % aqueous solution of **1** at room temperature in the presence of 5 wt % Rh/Al_2O_3 (1.1 mol% Rh). The rate of H_2-release was controlled by both the catalyst loadings and temperature.

Introduction

Owing to their high hydrogen densities, boron-based compounds, such as sodium borohydride ($NaBH_4$) and ammonia borane (NH_3BH_3), are now being intensively investigated as chemical hydrogen storage materials that can release hydrogen by either hydrolytic[1,2] or thermolytic processes.[3]

The high hydrogen release capacity that could potentially be achieved by ammonia triborane oxidative-hydrolysis, eq 1, (9.7 materials wt % H_2) or thermolysis, eq 2, (17.7 materials wt % H_2) also makes it an attractive candidate for chemical hydrogen storage.

$$NH_3B_3H_7 + 6H_2O \rightarrow NH_4^+ + 3BO_2 + 2H^+ + 8H_2 \quad (1)$$

$$NH_3B_3H_7 \rightarrow \text{“}B_3N\text{”} + 5H_2 \quad (2)$$

Although Kodama first synthesized[4] $NH_3B_3H_7$ over 50 years ago, owing to the lack of a suitable method for its efficient and safe synthesis, its reactivities and properties have not been intensively explored. Of the fewer than 30 previous publications on **1**, many were stimulated by the apparent contradiction between the computational studies[5] that predict a symmetric single hydrogen-bridged C_S-symmetric structure, and the early single crystal X-ray determination[6] of **1** that showed an asymmetric structure with perhaps two bridging-hydrogens.

In this paper we present (1) a new, efficient preparation of **1** that now makes this compound easily available; (2) a new crystallographic study of the solid-state structure of **1**, along with a structural determination of the **1**·18-crown-6 adduct, that

(1) For examples of $NaBH_4$ hydrolytic H_2-release reactions, see: (a) Amendola, S. C.; Sharp-Goldman, S. L.; Janjua, M. S.; Kelly, M. T.; Petillo, P. J.; Binder, M. *J. Power Sources* **2000**, *85*, 186–189. (b) Amendola, S. C.; Sharp-Goldman, S. L.; Janjua, M. S.; Spencer, N. C.; Kelly, M. T.; Petillo, P. J.; Binder, M. *Int. J. Hydrogen Energy* **2000**, *25*, 969–975. (c) Kojima, Y.; Suzuki, K.; Fukumoto, K.; Sasaki, M.; Yamamoto, T.; Kawai, Y.; Hayashi, H. *Int. J. Hydrogen Energy* **2002**, *27*, 1029–1034. (d) Dong, H.; Yang, H.; Ai, X.; Cha, C. *Int. J. Hydrogen Energy* **2003**, *28*, 1095–1100. (e) Jeong, S. U.; Kim, R. K.; Cho, E. A.; Kim, H.-J.; Nam, S.-W.; Oh, I.-H.; Hong, S. -A.; Kim, S. H. *J. Power Sources* **2005**, *144*, 129–134. (f) Krishnan, P.; Yang, T.-H.; Lee, W.-Y.; Kim, C.-S. *J. Power Sources* **2005**, *143*, 17–23. (g) Wee, J.-H.; Lee, K.-Y.; Kim, S. H. *Fuel Process. Technol.* **2006**, *87*, 811–819.

(2) For examples of amineborane hydrolytic H_2-release reactions, see: (a) Kelly, H. C.; Marriott, V. B. *Inorg. Chem.* **1979**, *18*, 2875–2878. (b) Shvets, I. B.; Erusalimchik, I. G. *Elektrokhimiya* **1984**, *20*, 535–537. (c) D'Ulivo, A.; Onor, M.; Pitzalis, E. *Anal. Chem.* **2004**, *76*, 6342–6352. (d) Storozhenko, P. A.; Svitsyn, R. A.; Ketsko, V. A.; Buryak, A. K.; Ul'yanov, A. V. *Zh. Neorg. Khim.* **2005**, *50*, 1066–1071. (e) Chandra, M.; Xu, Q. *J. Power Sources* **2006**, *156*, 190–194. (f) Chandra, M.; Xu, Q. *J. Power Sources* **2006**, *159*, 855–860. (g) Xu, Q.; Chandra, M. *J. Power Sources* **2006**, *163*, 364–370. (h) Mohajeri, N.; Adebiyi, O.; Baik, J.; Bokerman, G.; T-Raissi, A. *Prepr. Pap.-Am. Chem. Soc., Div. Fuel Chem.* **2006**, *51*, 520–521. (i) Chandra, M.; Xu, Q. *J. Power Sources* **2007**, *168*, 135–142. (j) Cheng, F.; Ma, H.; Li, Y.; Chen, J. *Inorg. Chem.* **2007**, *46*, 788–794. (k) Mohajeri, N.; T-Raissi, A.; Adebiyi, O. *J. Power Sources* **2007**, *167*, 482–485. (l) Clark, T. J.; Whittell, G. R.; Manners, I. *Inorg. Chem.* **2007**, *46*, 7522–7527. (m) Kalidindi, S. B.; Indirani, M.; Jagirdar, B. R. *Inorg. Chem.* **2008**, *47*, 7424–7429. (n) Yan, J.-M.; Zhang, X.-B.; Han, S.; Shioyama, H.; Xu, Q. *Angew. Chem., Int. Ed.* **2008**, *47*, 2287–2289. (o) Yoon, C. W.; Sneddon, L. G. *J. Am. Chem. Soc.* **2006**, *128*, 13992–13993.

(3) For examples of amineborane thermolytic H_2-release reactions, see: Stephens, F. H.; Pons, V.; Baker, R. T. *Dalton Trans.* **2007**, 2613–2626, and references therein.

(4) (a) Kodama, G. *Ph.D. Dissertation* 1957, University of Michigan. (b) Kodama, G.; Parry, R. W. *Proc. XVI Int. Congress Pure Appl. Chem.* **1957**, 482–489. (c) Kodama, G.; Parry, R. W.; Carter, J. C. *J. Am. Chem. Soc.* **1959**, *81*, 3534–3538.

(5) (a) Brown, L. D.; Lipscomb, W. N. *Inorg. Chem.* **1977**, *16*, 1–7. (b) McKee, M. L. *Inorg. Chem.* **1988**, *27*, 4241–4245. (c) Mebel, A. M.; Musaev, D. G.; Morokuma, K. *Chem. Phys. Lett.* **1993**, *214*, 69–76. (d) Es-sofi, A.; Serrar, C.; Ouassas, A.; Jarid, A.; Boutalib, A.; Nebot-Gil, I.; Tomás, F. *J. Phys. Chem. A* **2002**, *106*, 9065–9070. (e) Nguyen, V. S.; Matus, M. H.; Nguyen, M. T.; Dixon, D. A. *J. Phy. Chem. C* **2007**, *111*, 9603–9613. (f) Subotnik, J. E.; Sodt, A.; Head-Gordon, M. *Phys. Chem. Chem. Phys.* **2007**, *9*, 5522–5530. (g) Sundberg, M. R.; Sanchez-Gonzalez, A. *Inorg. Chem. Commun.* **2007**, *10*, 1229–1232.

(6) Nordman, C. E.; Reimann, C. *J. Am. Chem. Soc.* **1959**, *81*, 3538–3543.

resolves the contradictions with computational structural predictions; and (3) a description of the hydrolytic hydrogen release properties of **1**.

Experimental Section

All manipulations were carried out using standard high-vacuum or inert-atmosphere techniques as described by Shriver.[7]

Materials. Aldrich $NaBH_4$ (98%), iodine, 18-crown-6, $RhCl_3$, $[Rh(COD)(\mu\text{-}Cl)]_2$ (COD = 1,5-cyclooctadiene), Pd/Al_2O_3, Pt/C, Pt (nanosize, activated), Pd (sub-micrometer), Ru powder, and $NiCl_2$ from Aldrich or Strem Rh/Al_2O_3, Ru/Al_2O_3, and $RuCl_3$ were stored under inert atmosphere and used as received. Diglyme (Acros Organics) was distilled over Na prior to use. Glyme, dimethoxyethane, (Aldrich) was dried by passing through an activated alumina column prior to use. $Bu_4N^+B_3H_8^-$ was prepared according to the procedure described by Ryschkewitsch.[8]

Physical Measurements. ^{11}B NMR spectra at 128.4 MHz and ^1H NMR spectra at 400.1 MHz were obtained on a Bruker DMX-400 spectrometer equipped with appropriate decoupling accessories. ^1H NMR spectra at 500.1 MHz were obtained on a Bruker AM-500 spectrometer. All ^{11}B chemical shifts are referenced to external $BF_3{\cdot}O(C_2H_5)_2$ (0.0 ppm) with a negative sign indicating an upfield shift. All ^1H chemical shifts were measured relative to internal residual protons from the lock solvents (99.9% CD_2Cl_2 or 99.5% C_6D_6) and are referenced to $(CH_3)_4Si$ (0.0 ppm). Diffuse reflectance infrared Fourier transform (DRIFT) spectra were obtained on a Perkin-Elmer 100 FT-IR spectrometer with DRIFT accessory. Melting points were determined using a standard melting point apparatus and are uncorrected. All pH measurements were performed using an Orion 230 pH meter.

Preparation of $NH_3B_3H_7$ (1) from $Bu_4N^+B_3H_8^-$. After a solution of $Bu_4N^+B_3H_8^-$ (1.0 g, 3.53 mmol) in dry glyme (10.0 mL) was cooled at −70 °C for 15 min under an inert atmosphere, a solution of iodine (0.44 g, 1.73 mmol) in dry glyme (10.0 mL) was added, and the resulting solution stirred for 10 min at this temperature. The reaction mixture was then allowed to warm to room temperature, during which time the purple color of the solution faded, indicating consumption of the I_2. Analysis of the solution by ^{11}B NMR showed the formation of $(glyme)B_3H_7$. The solution was again cooled at −70 °C and anhydrous ammonia was bubbled through the solution with vigorous stirring. The solution was then warmed slowly to room temperature, and the white precipitate that had formed was removed by filtration. The filtrate was dried in vacuo and separation of the resulting residue by silica gel chromatography with CH_2Cl_2 as an eluent gave a white crystalline powder, $NH_3B_3H_7$ (0.16 g, 2.83 mmol) in 80% yield. The melting point and spectroscopic data match the literature values for $NH_3B_3H_7$.[9] Mp ≈ 73 °C. ^1H NMR (400.13 MHz, CD_2Cl_2) 3.58 (t, 3, N*H*$_3$), 1.62 (br, 7, B$_3$*H*$_7$). ^{11}B NMR (128.4 MHz, CD_2Cl_2) −7.7 (br, s, 2, *B2* and *B3*), −32.8 (br, s, 1, *B1*). IR (cm^{-1}) 3321(m), 3251(w), 2494(s), 2435(s), 1599(m), 1388(s), 1164(m), 1122(w), 1011(w), 882(w).

The reaction residue after the ammonia treatment could be alternatively purified by sublimation at 50 °C under reduced pressure, but this method took longer and afforded lower yields (<50%). (***CAUTION:*** *after sublimation, immediate deactivation of the oily residue is required; otherwise the residue and/or gases from the oily residue can enflame upon exposure to air*).

Table 1. Crystallographic Data Collection and Structure Refinement Information

	1	**1**·18-crown-6
empirical formula	$B_3H_{10}N$	$C_{12}B_3H_{34}NO_6$
fw	56.52	320.83
cryst class	monoclinic	monoclinic
space group	$P2_1/n$ (no. 14)	$P2_1/n$ (no. 14)
Z	4	8
a, Å	10.358(3)	21.961(3)
b, Å	4.8041(12)	8.5678(9)
c, Å	9.967(3)	21.910(3)
β, deg	115.141(6)	113.555(3)
V, Å^3	448.9(2)	3779.1(8)
D_{calc}, g/cm^3	0.836	1.128
μ, cm^{-1}	0.41	0.83
λ, Å (Mo K)	0.71073	0.71073
cryst size, mm	0.44 × 0.30 × 0.20	0.42 × 0.12 × 0.10
F(000)	128	1408
2θ angle, deg	7.48−50.00	5.16−50.02
T, K	143	143
hkl collected	$-12 \le h \le 12$	$-25 \le h \le 26$
	$-5 \le k \le 4$	$-10 \le k \le 7$
	$-11 \le l \le 11$	$-22 \le l \le 26$
no. reflections measured	3496	22 010
no. unique reflns	791 (R_{int} = 0.0201)	6590 (R_{int} = 0.0420)
no. observed reflns ($F > 4\sigma$)	722	5869
no. reflections used in refinement	791	6590
no. of params	78	671
R^a indices	R1 = 0.0411	R1 = 0.0498
($F > 4\sigma$)	wR2 = 0.1078	wR2 = 0.1208
R^a indices	R1 = 0.0438	R1 = 0.0560
(all data)	wR2 = 0.1098	wR2 = 0.1270
GOF^b	1.091	1.086
final difference peaks, e/Å^3	+0.159, −0.173	+0.237, −0.258

^{a} $R1 = \Sigma||F_o| - |F_c||/\Sigma|F_o|$; $wR2 = \{\Sigma w(F_o^2 - F_c^2)^2/\Sigma w(F_o^2)^2\}^{1/2}$. ^{b} $GOF = \{\Sigma w(F_o^2 - F_c^2)^2/(n-p)\}^{1/2}$; n = the number of reflections; p = the number of parameters refined.

Computational Studies. DFT/GIAO/NMR calculations were performed using the Gaussian 03 program.[10a] The geometries were fully optimized at the B3LYP/6-31G(d) level without symmetry constraints. A vibrational frequency analysis was carried out on each optimized geometry using the same level of theory with a true minimum found for each structure (i.e., possessing no imaginary frequencies). The energies of the optimized structures of **1**, $MeNH_2B_3H_7$, and $Me_2NHB_3H_7$ and their corresponding dimers were computed both at the B3LYP/6-311+G(2d,p) level and at the MP2/6-311+G(2d,p) level based on the B3LYP/6-31G(d) optimized structures. In all cases, zero point energies obtained at the B3LYP/6-31G(d) level were scaled by 0.9804[10b] and then used for the final energy correction.

The ^{11}B NMR chemical shifts were calculated at the B3LYP/6-311G(d) level using the GIAO option within Gaussian 03. The ^{11}B NMR GIAO chemical shifts are referenced to $BF_3{\cdot}OEt_2$ using an absolute shielding constant of 101.58, which was obtained from the GIAO NMR calculated shift of $BF_3{\cdot}OEt_2$ at the B3LYP/6-311G(d)//B3LYP/6-31G(d) level of theory.

Crystallographic Data. Single crystals of **1** (Penn 3323) were obtained from a concentrated toluene solution stored at −20 °C. Crystals of the **1**·18-crown-6 ($C_{12}H_{24}O_6$) adduct (Penn 3304) were grown from 1:1 mixtures of **1** and 18-crown-6 in THF/hexanes at room temperature.

Collection and Reduction of the Data. Crystallographic data and structure refinement information are summarized in Table 1. X-ray intensity data were collected on a Rigaku Mercury CCD area detector employing graphite-monochromated Mo Kα radiation (λ = 0.71073 Å). Preliminary indexing was performed from a series of 12 0.5° rotation images with exposures of 30 s. Rotation images were processed using CrystalClear,[11a] producing a listing of unaveraged F^2 and $\sigma(F^2)$ values which were then passed to the CrystalStructure[11b] program package for further processing and

(7) Shriver, D. F.; Drezdon, M. A. *Manipulation of Air Sensitive Compounds*, 2nd ed.; Wiley: New York, 1986.
(8) (a) Nainan, K. C.; Ryschkewitsch, G. E. *Inorg. Nucl. Chem. Lett.* **1970**, *6*, 765–766. (b) Ryschkewitsch, G. E.; Nainan, K. C. *Inorg. Synth.* **1974**, *15*, 113–114.
(9) Dodds, A. R.; Kodama, G. *Inorg. Chem.* **1976**, *15*, 741–743.
(10) (a) Frisch, M. J. et al. *Gaussian 03*, Revision B.05; Gaussian, Inc.: Pittsburgh, 2003. (b) Foresman, J. B. and Frisch, E. *Exploring Chemistry with Electronic Structure Methods*, 2nd ed.; Gaussian, Inc.: Pittsburgh, 1996; p 64.
(11) (a) CrystalClear: Rigaku Corporation, 1999. (b) Crystal Structure: Crystal Structure Analysis Package, Rigaku Corp. Rigaku/MSC, 2002.

structure solution on a Dell Pentium III computer. The intensity data were corrected for Lorentz and polarization effects and for absorption.

Solution and Refinement of the Structure. The structures were solved by direct methods (SIR97).[12] Refinements were made by full-matrix least-squares based on F^2 using SHELXL-97.[13] All reflections were used during refinement (F^2's that were experimentally negative were replaced by $F^2 = 0$). Non-hydrogen atoms were refined anisotropically and hydrogen atoms were refined isotropically.

General Procedures for Hydrolytic H_2-Release Measurements from Aqueous $NH_3B_3H_7$ Solutions. Samples of **1** were added to neutral water in a two-necked round-bottom flask equipped with a sidearm containing acid or metal catalysts. The flask was connected to a gas buret via the second arm, closing the system. When the sidearm was inverted, the acid or catalyst was mixed with the aqueous $NH_3B_3H_7$ solution and H_2 was evolved. The volume of evolved H_2 was quantitatively measured versus time employing the gas buret with pressure equalization against atmospheric pressure. For the reactions at 30 and 50 °C, the final volumes were measured after cooling the reaction mixtures to room temperature.

Stability of Solid and Aqueous Ammonia Triborane. Solid **1** stored in air at room temperature showed no changes by ^{11}B NMR analysis after 2 months. The stability of a 33 wt % (8.8 M) aqueous solution (prepared by dissolving 0.33 g of **1** in 0.66 mL of distilled water) of **1** was determined by comparing the integration ratio of **1** (−32.9 ppm) and its NH_3BH_3 (−22.0 ppm) decomposition product in the ^{11}B NMR spectra taken versus time (Table S1).

For the 0.5 wt % solutions (0.09 M) with various pH values, a series of 10.0 mg samples of **1** were dissolved in 2.0 mL of distilled water or the desired buffers. The initial pH of the unbuffered **1** (0.5 wt %) solution was 8.7 by pH meter. The phosphate buffers (sodium dihydrogenphosphate, 99%, Aldrich) of 1.0 M concentrations were prepared by dissolving 12.0 g of NaH_2PO_4 and 14.6 g of NaCl in 90.0 mL of CO_2-free distilled water in a volumetric flask, and then adjusting the solution to the desired pH's using a minimum amount of HCl and/or NaOH. Additional CO_2-free distilled water was added into the volumetric flask to 100.0 mL. The degree of degradation of **1** was again measured by integrating the ratio of **1** and NH_3BH_3 in the ^{11}B NMR spectrum at each time (Table S1).

Hydrolysis of 1 with HCl. Concentrated HCl (11.8 N, 1.0 mL) was added to solid **1** (12.0 mg, 0.212 mmol) at room temperature, and the evolved hydrogen was quantitatively measured versus time with the gas buret (Table S2). In separate experiments, 1.9 mL of each of the standardized 0.93 (1.0 equiv), 2.79 (3.0 equiv), and 4.66 M (5.0 equiv) solutions of HCl was added to the three samples of **1** (0.1 g, 1.77 mmol) and the released hydrogen was quantitatively measured versus time with the gas buret (Table S3).

Hydrolysis of 1 with Metal Catalysts. Experiments were carried out at room temperature by adding the desired amounts (Table S4) of the metal catalysts to samples of **1** dissolved in neutral water (1.0 or 2.0 mL) and then measuring the evolved hydrogen versus time with the gas buret (Table S5).

Extended Catalyst Lifetime Studies of $[Rh(COD)(\mu\text{-}Cl)]_2$ (22.7 and 7.9 mol %) in the Absence of Buffer Solutions. The $[Rh(COD)(\mu\text{-}Cl)]_2$ (12 mg, 0.024 mmol, 22.9 mol %) precatalyst was added to 1.0 mL of the neutral water containing 4.6 mg (0.081 mmol) of **1** and the evolved H_2 was measured with the gas buret. More **1** was then added to the solution at four additional times, and the evolved hydrogen measured (Table S6). In a separate experiment, the $[Rh(COD)(\mu\text{-}Cl)]_2$ (3.6 mg, 0.0073 mmol, 7.9 mol %) catalyst was added to 1.0 mL of neutral water containing 4.8 mg (0.085 mmol) of **1**. More **1** was then added to the solution at three additional times and the evolved hydrogen measured (Table S7).

Extended Catalyst Lifetime Studies of 5 wt % Rh/Al_2O_3 (7 mol % Rh) in the Presence of Buffer Solutions. A borate-buffered solution was prepared by adding CO_2-free distilled water to a volumetric flask containing 3.05 g of $Na_2B_4O_7 \cdot 10H_2O$ and then adjusting the pH of the solution to 7.2. The 5 wt % Rh/Al_2O_3 (1.25 mg Rh, 0.0121 mmol Rh) catalyst was added to 2.0 mL of the buffer solution containing 9.0 mg (0.159 mmol) of **1** and the evolved H_2 was measured with the gas buret. More **1** was periodically added to the solution at 10 additional times and the evolved hydrogen measured (Table S8).

Hydrolysis of 1 with Rh/Al_2O_3 at Different Temperatures. In separate experiments, 40 mg samples of Rh/Al_2O_3 (5 wt % Rh/Al_2O_3, 0.019 mmol Rh, 1.1 mol % Rh) were added to 4.9 wt % aqueous solutions of **1** (0.1 g $NH_3B_3H_7$ + 1.9 mL H_2O + 40 mg Rh/Al_2O_3) at 0, 20, 35, and 50 °C and the evolved hydrogen was then measured versus time (Table S9).

Hydrolysis of a Concentrated Aqueous $NH_3B_3H_7$ Solution. A 40 mg sample of Rh/Al_2O_3 (5 wt % Rh/Al_2O_3, 0.019 mmol Rh, 1.1 mol % Rh) was added to a 22.7 wt % aqueous solution of **1** (0.1 g $NH_3B_3H_7$ + 0.3 mL H_2O + 40 mg Rh/Al_2O_3) at room temperature. The evolved hydrogen was quantitatively measured versus time with the gas buret (Table S10). The weight percent of the hydrogen produced was calculated by materials wt % H_2 released = [H_2 wt produced/($NH_3B_3H_7$ + H_2O + Rh/Al_2O_3 wts)] × 100.

Results and Discussion

Synthesis. Kodama[4] originally synthesized ammonia triborane (**1**) by a two-step process (eqs 3 and 4) involving (1) the cleavage reaction of tetraborane, B_4H_{10}, with ethers to initially form LB_3H_7 (L = tetrahydrofuran or tetrahydropyran) adducts (plus B_2H_6), followed by (2) displacement of the ethers by reaction with anhydrous ammonia. Unfortunately, since tetraborane is both thermally unstable and explosive in air, a large-scale synthesis based on this method is not feasible.

$$B_4H_{10} + L \rightarrow LB_3H_7 + 1/2B_2H_6 \quad (3)$$

$$LB_3H_7 + \text{anhydrous } NH_3 \rightarrow NH_3B_3H_7 + L \quad (4)$$

Kodama also showed **1** could be obtained from the reaction of $Na^+B_3H_8^-$ with NH_4Cl, but in much lower yields (typically 20−30%) than the tetraborane-based route. The air- and moisture-stable $B_3H_8^-$ anion is an attractive starting material since it can be readily made by the iodine oxidation of sodium borohydride (eq 5).[8] Binder[14] previously reported that I_2 oxidation of $Me_4N^+B_3H_8^-$ in noncoordinating solvents (e.g., CH_2Cl_2) yielded the B_3H_7 dimer, B_6H_{14}. We found that iodine oxidation (with slow warming from −70 to 20 °C) of the air-stable $Bu_4N^+B_3H_8^-$ salt in glyme (1,2-dimethoxyethane) provided an efficient method for preparing solutions of the (glyme)B_3H_7 adduct (eq 6).

$$3Na^+BH_4^- + I_2 \xrightarrow[110°C]{\text{diglyme}} Na^+B_3H_8^- + 2NaI + 2H_2 \quad (5)$$

$$NBu_4{}^+B_3H_8^- + 1/2I_2 \xrightarrow[-70-23°C]{\text{glyme}} (\text{glyme})B_3H_7 + 1/2H_2 + NBu_4I \quad (6)$$

$$(\text{glyme})B_3H_7 + NH_3(g) \xrightarrow[-70-23°C]{\text{glyme}} NH_3B_3H_7 + \text{glyme} \quad (7)$$

(12) Altomare, A.; Burla, M.; Camalli, M.; Cascarano, G.; Giacovazzo, C.; Guagliardi, A.; Moliterni, A.; Polidori, G.; Spagna, R. *J. Appl. Crystallogr.* **1999**, *32*, 115–119.

(13) Sheldrick, G. M. *SHELXL-97: Program for the Refinement of Crystal Structures*; University of Göttingen: Göttingen, Germay, 1997.

(14) Brellochs, B.; Binder, H. *Angew. Chem., Int. Ed. Engl.* **1988**, *27*, 262–3.

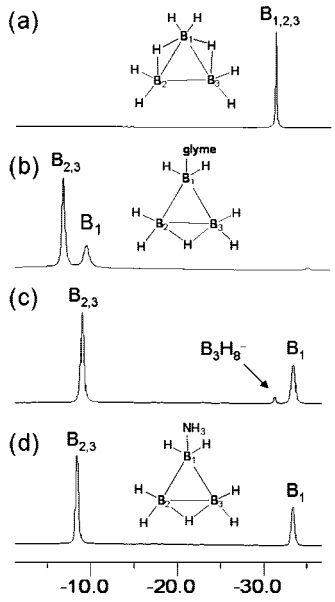

Figure 1. $^{11}B\{^1H\}$ NMR spectra for the reaction progression leading to the formation of **1**: (a) $B_3H_8^-$, (b) (glyme)B_3H_7 formed after I_2 oxidation of $B_3H_8^-$ in glyme, (c) **1** formed following ammonia displacement of the coordinated glyme (before purification), and (d) **1** after silica gel filtration.

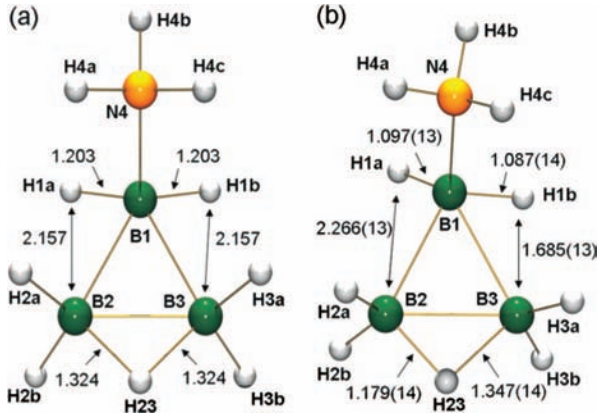

Figure 2. (a) DFT (B3LYP/6-31G(d)) optimized structure of **1** and (b) crystallographically redetermined structure of **1**.

As shown in Figure 1, upon treatment with iodine at low temperature, the $B_3H_8^-$ anion was oxidized to give a new compound that exhibited broad ^{11}B NMR resonances in a 2:1 ratio at −6.8 and −9.5 ppm, respectively, in agreement with the DFT/GIAO calculated chemical shifts for (glyme)B_3H_7, −3.6 (B2,3) and −11.1 ppm (B1). Treatment of the glyme solution with anhydrous ammonia at −70 °C then afforded **1**. Any unreacted $B_3H_8^-$ was easily removed by filtration of the reaction solution through silica gel to give pure **1** in 80% yield. **1** could also be purified by vacuum sublimation at 50 °C, but some decomposition occurred lowering the yield to less than 50%. All spectroscopic data for **1** are in agreement with the literature values.[9]

Structural Studies. There have been a number of computational studies that have predicted that **1** should have a C_S-symmetric structure with a single bridging hydrogen.[5] The DFT-optimized geometry along with selected bond distances for this structure is shown in Figure 2a. In this structure, both H1a and H1b are bound only to B1, and the H23 bridging hydrogen is symmetrically located on the B2−B3 edge.

In contrast to the computationally predicted structures, the early X-ray crystallographic determination reported[6] by Nordman and Reimann (NR) showed that **1** is highly distorted in the solid-state with H1b located between B1 and B3, and with H23 in an asymmetric position closer to B2 than B3. NR suggested that **1** has a structure close to a double bridging hydrogen conformation, but with the caveat that the single bridging-hydrogen conformation shown in Figure 2a could not be entirely excluded. The fact that the NR data were not of sufficient quality to allow location of the NH_3 hydrogen positions also raises uncertainty about structural conclusions based on their determination.

In order to help resolve the inconsistency between the computational predictions and the NR structure, we redetermined the structure of **1**. The higher quality of the diffraction data in this redetermination enabled the location and refinement of all hydrogens. As shown in Figure 2b, the geometrical parameters for the redetermined structure are, in fact, consistent with those of the original NR structure but reveal an even more asymmetric geometry, with H1b closer to B3, (B3−H1b, 1.685(13) Å), than was found in the NR structure, (1.75(3) Å). This B3−H1b distance is likewise much shorter than B2−H1a (2.266(13) Å), causing the H1b−B1−B3 (66.0(7)°) angle to be much more acute than H1a−B1−B2 (99.1(7)°), clearly indicating interactions between B3 and H1b. Consistent with this interpretation, B1−B3 (1.798(2) Å) is shorter than B1−B2 (1.819(2) Å) but longer than B2−B3 (1.743(2) Å). Also as in the NR structure, H23 is asymmetrically positioned between B2 and B3 with B3−H23 (1.347(14) Å) being significantly longer than B2−H23 (1.179(14) Å). Therefore, in agreement with the previous NR structure, the solid-state structure of **1** has a triborane unit with a second partially hydrogen-bridging conformation, rather than the computationally predicted single hydrogen-bridged structure.

A comparison of the bond distances and angles for the DFT-optimized geometry of **1** with those of the redetermined structure is given in the first two columns of Table 2, where it is apparent that there are substantial differences in the two structures, not only in the distances and angles involving H1b and H23, but also with the B1−N (1.642 vs 1.585(2) Å); B1−B2 (1.849 vs 1.819(2) Å) and B1−B3 (1.849 vs 1.798(2) Å) distances, as well as the B3−B1−N (108.1° vs 115.28(9)°) angle.

When the molecular geometry observed in the crystal structure of **1** was computationally optimized at B3LYP/6-31G(d), it reverted to that of the symmetric single-bridged structure in Figure 2a. The question that then arises is: Why is the solid-state structure of **1** significantly different from that of the computationally predicted structure?

Crabtree[15] has shown that intermolecular dihydrogen bonding between hydridic B−H (δ^-) and protonic N−H (δ^+) hydrogens is important for "BNH" compounds. The B−H···H−N dihydrogen bonding distances are typically ∼1.7−2.2 Å, and, in contrast to classical hydrogen-bonding interactions, the B−H···H−N unit is not linear, with the H−H−N angles usually larger, 117−171°, than the B−H−H angles, 95−120°.

The ORTEP plot presented in Figure 3a shows the relative orientation of the molecular units in the solid-state crystal structure of **1**, where it can be seen that the three ammonia N−H

(15) (a) Richardson, T. B.; de Gala, S.; Crabtree, R. H. *J. Am. Chem. Soc.* **1995**, *117*, 12875–12876. (b) Crabtree, R. H.; Siegbahn, P. E. M.; Eisenstein, O.; Rheingold, A. L.; Koetzle, T. F. *Acc. Chem. Res.* **1996**, *29*, 348–354. (c) Klooster, W. T.; Koetzle, T. F.; Siegbahn, P. E. M.; Richardson, T. B.; Crabtree, R. H. *J. Am. Chem. Soc.* **1999**, *121*, 6337–6343.

Table 2. Comparisons of Selected Bond Distances (Å) and Angles (deg) from the DFT-Optimized Geometry of **1**, the Crystallographically Redetermined Structure of **1**, the Crystal Structure of **1**·18-Crown-6 (Molecule a), and the DFT-Optimized Geometry of **1**·18-Crown-6 (Molecule a)

parameters	**1** (DFT)	**1** (exptl)	**1**·18-crown-6 (exptl)	**1**·18-crown-6 (DFT)
B1−N	1.642	1.585(2)	1.582(3)	1.607
B1−B2	1.849	1.819(2)	1.829(4)	1.857
B1−B3	1.849	1.798(2)	1.842(4)	1.859
B2−B3	1.729	1.743(2)	1.725(5)	1.725
B2−H23	1.324	1.179(14)	1.33(3)	1.335
B3−H23	1.324	1.347(14)	1.27(3)	1.321
B1−H1a	1.203	1.097(13)	1.12(3)	1.211
B1−H1b	1.203	1.106(14)	1.09(3)	1.209
B3−H1b	2.157	1.685(13)	2.192(26)	2.176
B2−H1a	2.157	2.266(13)	1.933(26)	2.091
B2−H2a	1.208	1.087(14)	1.05(3)	1.204
B2−H2b	1.195	1.105(14)	1.14(2)	1.199
B3−H3a	1.208	1.080(14)	1.14(3)	1.205
B3−H3b	1.195	1.085(14)	1.09(3)	1.199
N−H4a	1.022	0.87(2)	0.98(3)	1.026
N−H4b	1.021	0.91(2)	0.95(3)	1.026
N−H4c	1.022	0.87(2)	0.81(3)	1.025
B2−B1−B3	55.8	57.61(7)	56.1(2)	55.3
B1−B2−B3	62.1	60.58(7)	62.4(2)	62.4
B1−B3−B2	62.1	61.81(7)	61.6(2)	62.3
B2−B1−N	108.1	110.98(9)	113.7(2)	112.6
B3−B1−N	108.1	115.28(9)	110.0(2)	111.5
B2−H23−B3	81.6	87.0(9)	83.0(5)	81.0
H23−B2−B3	49.2	50.5(7)	46.8(12)	49.1
H23−B3−B2	49.2	42.5(6)	50.1(13)	49.9
H1a−B1–B2	87.3	99.1(7)	78.0(14)	83.1
H1b−B1–B3	87.3	66.0(7)	93.4(14)	87.6
H4a−O1	–	–	2.011(28)	2.027
H4b−O3	–	–	2.068(22)	2.043
H4c−O5	–	–	2.195(23)	2.046

hydrogens are each directed toward different B−H hydrogens on adjacent triborane fragments, thus suggesting the possibility of significant intermolecular B−H···H−N dihydrogen bonding interactions. The schematic diagram in Figure 3b provides more details of the intermolecular interactions between the ammonia hydrogens, H4a, H4b, and H4c, of a central $NH_3B_3H_7$ and the nearest B−H hydrogens, H1a, H2b, and H3a, on adjacent B_3H_7 fragments.

The H4b−H2b distance (2.13(3) Å) and the N−H4b−H2b (146(2)°) and H4b−H2b−B2 (123(1)°) bond angles are all within the ranges previously found for molecules having strong B−H···H−N dihydrogen bonding interactions. The H4b−H2b distance is slightly longer than the closest N−H···H−B distance (2.02(3) Å)[15c] found in the neutron diffraction study of the solid-state NH_3BH_3 structure. On the other hand, while having bent B−H···H and H···H−N angles typical of dihydrogen bonding values, the H1a−H4a (2.41(2) Å) and H4c−H3a (2.43(2) Å) distances are close to normal nonbonding H···H contacts (>2.4 Å), suggesting only weak interactions between these hydrogens.

These observations suggest that dihydrogen bonding of the H4b and H2b hydrogens may give rise to the distorted solid-state structure of **1**. That is, the H4b−H2b interaction may weaken the bonding between H2b and B2 and thereby enhance B2−H23 bonding resulting in the shortening of B2−H23 (1.179(14) Å) and elongation of B3−H23 (1.347(14) Å). This change could then induce a new bonding interaction between B3 and H1b that results in a shortening of B3−H1b (1.685(13) Å) compared to B2−H1a (2.266(13) Å).

The stabilizing effects of these intermolecular interactions are not included in the molecular gas-phase structural calculations of **1**; therefore, such computations yield the C_S-symmetric

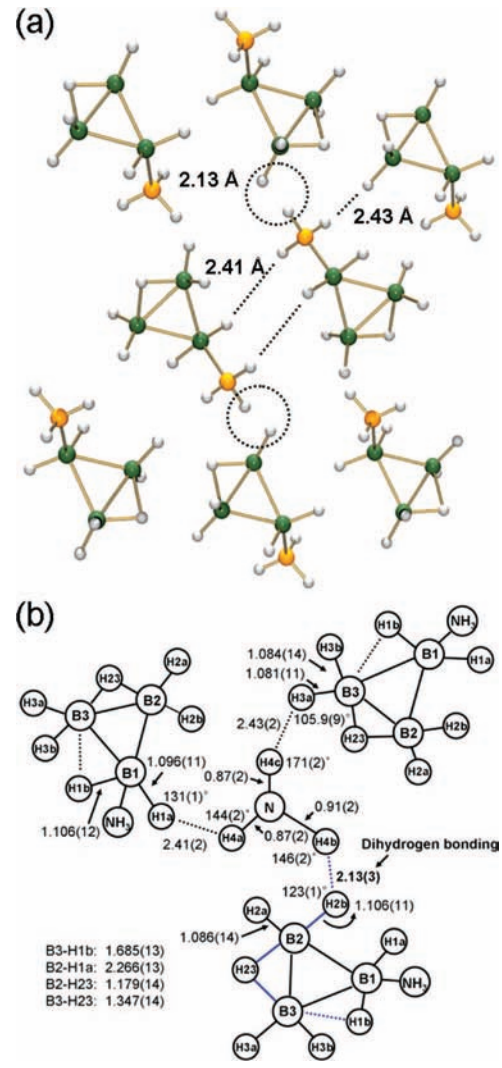

Figure 3. (a) ORTEP view showing the relative orientation of the molecular units and potential intermolecular B−H···H−N interactions in the solid-state structure of **1** and (b) a schematic diagram showing the closest intermolecular interactions in the solid-state structure of **1**.

structure as lowest energy. In order to provide computational support for the effects of intermolecular dihydrogen bonding on the solid-state structure of **1**, several dimeric structures that might serve as models for the types of intermolecular interactions observed in the solid state were optimized by DFT at B3LYP/6-31G(d). Two energetically favored dimeric structures were located (Figure 4). The lower energy side-by-side structure $\mathbf{1_2}$ shows, as found in the solid-state structure of **1**, dimeric interactions (1.97 Å) between one of the terminal hydrogens on B2 (but, in this case H2a′ instead of H2b) and one hydrogen on the NH_3 (but, in this case H4a′ instead of H4b) with the bent B2′−H2a′−H4a′ (100.5°) and H2a′−H4a′−N4′ angles (142.2°) again in the ranges observed for dihydrogen-bonding. The 1.97 Å dihydrogen distance is somewhat longer than was found in the PCI-80/B3LYP computational study[15a] of dihydrogen bonding in NH_3BH_3 dimers (1.82 Å). The MP2/6-311+G(2d,p) calculated 11.0 kcal/mol stabilization of $\mathbf{1_2}$ relative to 2 equiv of **1** (2.5 kcal/mol at B3LYP/6-311+G(2d,p)) is similar to that found for the NH_3BH_3 dimer (12.1 kcal/mol)[15a] at PCI-80/B3LYP. Even with the four (but longer) dihydrogen interactions, the face-to-face dimer $\mathbf{1_2}'$ (Figure 4b) was found to be 1.3 kcal/mol less stable than $\mathbf{1_2}$.

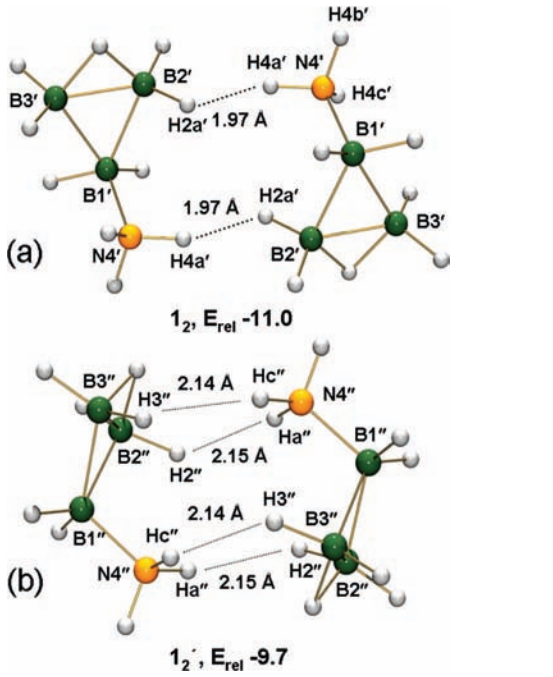

Figure 4. B3LYP-optimized dimeric structures of **1**: (a) $\mathbf{1}_2$ and (b) $\mathbf{1}_2'$. The MP2/6-311+G(2d,p)-calculated energies are in kcal/mol and are based on the B3LYP/6-31G(d)-optimized structures relative to two separated $NH_3B_3H_7$ molecules. Selected intermolecular distances and angles. $\mathbf{1}_2$: H2a′−H4a′, 1.97 and 1.97 Å; B2−H2a′−H4a′, 100.5° and 100.5°; H2a′−H4a′−N4′, 142.2° and 142.2°. $\mathbf{1}_2'$: H2″−Ha″, 2.15 and 2.15 Å; H3″−Hc″, 2.14 and 2.14 Å; B2″−H2″−Ha″, 118.9° and 119.4°; H2″−Ha″−N4″, 146.0° and 146.4°; B3″−H3″−Hc″, 118.9° and 118.9°; H3″−Hc″−N4″, 146.7° and 147.0°.

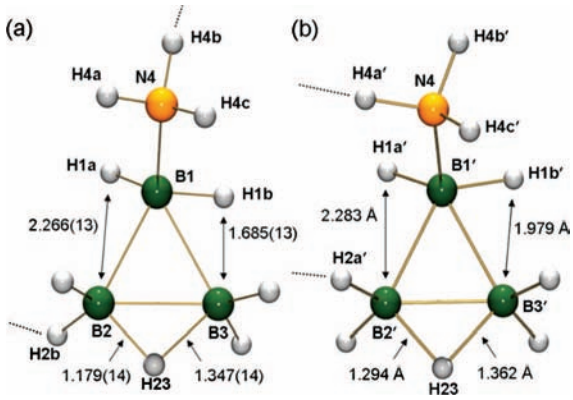

Figure 5. Comparison of (a) the solid-state structure of **1** with (b) the DFT-optimized $\mathbf{1}_2$ structure. Dashed lines indicate the positions of the dihydrogen bonding interactions.

While $\mathbf{1}_2'$ exhibited a nearly C_S-symmetric $NH_3B_3H_7$ framework with a single-bridging hydrogen on each triborane fragment, it is significant, as illustrated in Figure 5 and Table 3 that the lower energy structure $\mathbf{1}_2$ had an asymmetric structure that resembles the observed solid-state structure of **1**, with both H1b moving closer to B3, and H23 moving away from B3 toward B2 such that it is asymmetrically bonded at the B2−B3 edge. Likewise, the B2−B1−N (107.42°) and B3−B1−N (112.23°) angles are not equivalent.

Similar structural changes were computationally observed between the DFT-optimized monomeric structures of $MeNH_2B_3H_7$ and $Me_2NHB_3H_7$ and their dihydrogen-bonded dimers. As shown in Figure 6, the DFT-optimized structures of both $MeNH_2B_3H_7$ and $Me_2NHB_3H_7$ have only one hydrogen bridge that is located in a symmetric position across the B2−B3 edge. The computational studies identified two dimeric $(MeNH_2B_3H_7)_2$ (**Me-1₂**, −12.1 and **Me-1₂′**, −8.9 kcal/mol) and one dimeric $(Me_2NHBH_3)_2$ (**Me₂-1₂**, −12.8 kcal/mol) structures (Figure 7) that, as a result of their dihydrogen bonding interactions, (B−H···H−N distances: 1.98 Å, **Me-1₂**; 2.01 and 2.17 Å, **Me-1₂′**; 2.04 and 2.14 Å, **Me₂-1₂**) were more stable than 2 equiv of their respective monomers. As was the case for **1**, while the DFT geometry optimizations of the monomeric $MeNH_2B_3H_7$ and $Me_2NHB_3H_7$ structures yielded C_S-symmetric single hydrogen-bridging geometries, the optimized **Me-1₂** and **Me₂-1₂** structures exhibited asymmetric structures (Figure 8), similar to those of both $\mathbf{1}_2$ and the solid-state **1** structure, again confirming the structural consequences of intermolecular B−H···H−N dihydrogen bonding.

Table 3. Comparisons of Selected Bond Distances and Angles Observed in the Solid-State Structure of **1** with Those Calculated for the DFT-Optimized Structure of $\mathbf{1}_2$

	1	$\mathbf{1}_2$
B−N	1.585(2)	1.630
B1−B2	1.819(2)	1.843
B1−B3	1.798(2)	1.841
B2−B3	1.743(2)	1.729
B1−H1a	1.097(13)	1.201
B1−H1b	1.087(14)	1.208
B3−H1b	1.685(13)	1.979
B2−H1a	2.266(13)	2.283
B2−H23	1.179(14)	1.294
B3−H23	1.347(14)	1.362
B2−H2a	1.086(14)	1.208
B2−H2b	1.106(11)	1.202
B3−H3a	1.081(11)	1.203
B3−H3b	1.084(14)	1.194
N4−H4a	0.87(2)	1.027
N4−H4b	0.91(2)	1.021
N4−H4c	0.87(2)	1.022
B2−B1−B3	57.61(7)	55.99
B1−B2−B3	60.58(7)	61.96
B1−B3−B2	61.81(7)	62.05
B2−B1−N	110.98(9)	107.42
B3−B1−N	115.28(9)	112.23
B2−H23−B3	87.0(9)	81.20
H23−B2−B3	50.5(7)	51.10
H23−B3−B2	42.5(6)	47.70
H1a−B1−B2	99.1(7)	94.86
H1b−B1−B3	66.0(7)	77.87

Further evidence for the effects of intermolecular dihydrogen bonding on the solid-state structure of **1** comes from the

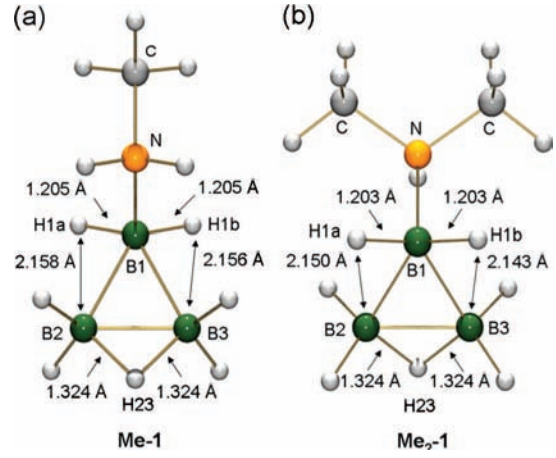

Figure 6. DFT-optimized structures of $MeNH_2B_3H_7$ (a, **Me-1**) and $Me_2NHB_3H_7$ (b, **Me₂-1**).

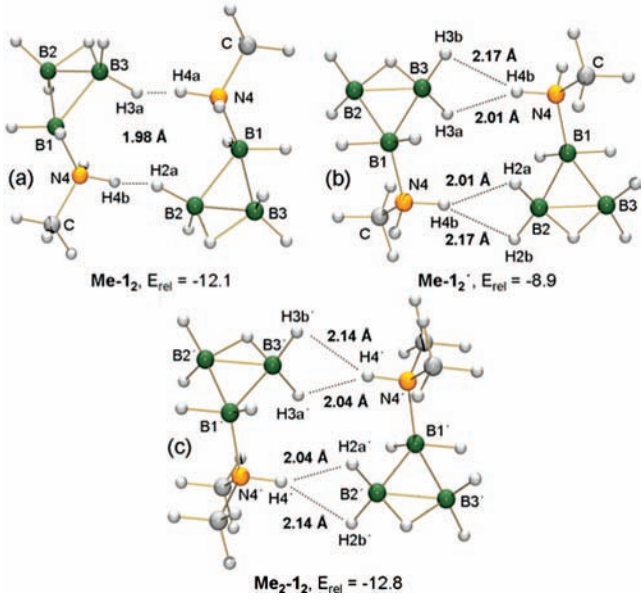

Figure 7. DFT-optimized dimeric structures of (a) $(MeNH_2B_3H_7)_2$, **Me-1$_2$**, (b) $(MeNH_2B_3H_7)_2$, **Me-1$_2$′**, and (c) $(Me_2NHB_3H_7)_2$, **Me$_2$-1$_2$**. The MP2/6-311+G(2d,p)-calculated energies are in kcal/mol and are based on the B3LYP/6-31G(d)-optimized structures relative to 2 equiv of $MeNH_2B_3H_7$ and $Me_2NHB_3H_7$, respectively.

structural determination of the **1**·18-crown-6 adduct. Ammonia borane has previously been shown to form NH_3BH_3·18-crown-6 adducts, where the three ammonia hydrogens are hydrogen-bonded to the 18-crown-6 oxygens.[16] We likewise found that the crystalline $NH_3B_3H_7$·18-crown-6 adduct formed from a THF/hexanes solution containing a 1:1 mixture of **1** and 18-crown-6 (eq 8).

$$NH_3B_3H_7 + \text{18-crown-6} \rightarrow \mathbf{1}\cdot\text{18-crown-6} \qquad (8)$$

A structural determination showed two independent molecules of **1**·18-crown-6 in the asymmetric unit, but since there were no significant differences in the two structures, only the structure of molecule a, given in Figure 9, is discussed. The ammonia hydrogens of the ammonia triborane unit each hydrogen bond to one of the oxygen atoms of the crown ether with the longest O−H distance (H4a−O1, 2.011(28) < H4b−O3, 2.068(22) < H4c−O5, 2.195(23) Å) correlating with the shortest N−H (N4−H4c (0.81(3) < N4−H4a (0.98(3) Å), N4−H4b (0.95(3) Å). As a result of these favored O···H−N hydrogen-bonding interactions, there are no B−H···H−N interactions less than 6.8 Å.

In contrast to the asymmetric structure observed in the solid-state structure of pure **1**, the ammonia triborane fragment in **1**·18-crown-6 has a much more symmetric single hydrogen-bridging framework that is more in line with the computational results for **1**. Moreover, unlike for **1**, the DFT-optimized structure of **1**·18-crown-6 (Figure 10 and Table 2) is in good agreement with the **1**·18-crown-6 crystallographic determination. In both the crystal and DFT-optimized structures, H23 is bonded in a symmetric fashion at the B2−B3 edge, and the long (>1.93 Å) H1a−B2 and H1b−B3 distances clearly indicate that H1a and H1b are bound only to B1. The slight asymmetry observed in both the crystal and DFT-optimized structures (e.g., H1a−B2 < H1b−B3) of **1**·18-crown-6 undoubtedly arises because of the asymmetric ammonia conformation that is dictated by its hydrogen-bonding interactions with the oxygen atoms of the 18-crown-6. Thus, in the absence of any significant B−H···H−N dihydrogen interactions, the ammonia triborane fragment in **1**·18-crown-6 adopts the single hydrogen-bridging conformation that is computationally favored for **1**.

(16) (a) Colquhoun, H. M.; Jones, G.; Maud, J. M.; Stoddart, J. F.; Williams, D. J. *J. Chem. Soc., Dalton Trans.* **1984**, 63–66. (b) Alston, D. R.; Stoddart, J. F.; Wolstenholme, J. B.; Allwood, B.; Williams, D. J. *Tetrahedron* **1985**, *41*, 2923–2926.

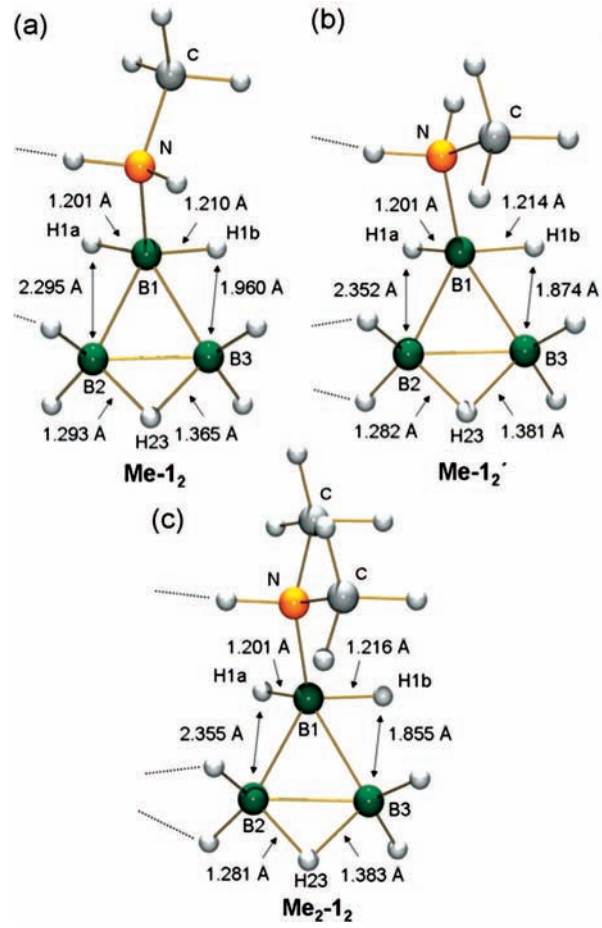

Figure 8. Selected bond distances in the model dimeric structures (a) $(MeNH_2B_3H_7)_2$, **Me-1$_2$**, (b) $(MeNH_2B_3H_7)_2$, **Me-1$_2$′**, and (c) $(Me_2NHB_3H_7)_2$, **Me$_2$-1$_2$** structures. The dashed lines indicate the positions of the dihydrogen bonding interactions.

Hydrolytic Hydrogen Release. As described earlier by eq 1, oxidative hydrolysis of **1** could release 8 equiv of H_2 making such a process potentially competitive with either $NaBH_4$ or NH_3BH_3 based hydrolytic H_2-release systems. Two factors that are critical for such applications are aqueous solubility and stability. In this regard, owing most probably to its N−H···O hydrogen-bonding properties discussed in the previous section, **1** proved to be remarkably soluble in water, with solutions of at least 33 wt % being attained. Furthermore unlike aqueous $NaBH_4$, which is stable only in strongly alkaline solutions,[1a,b] $NH_3B_3H_7$ was reasonably stable in neutral aqueous solutions, as evidenced by the ^{11}B NMR studies shown in Figure 11 of a 20 wt % solution of **1** which showed that, even after 11 days, only a small amount had decomposed to ammonia borane and borates. Likewise, in agreement with Kodama's previous report of the air stability of **1**,[4] ^{11}B NMR studies showed solid **1** stored in air was not changed even after 2 months at room temperature.

Efficient H_2-release from aqueous solutions of **1** was obtained upon the addition of either acids or appropriate metal catalysts. Acid hydrolysis of NH_3BH_3 has previously been demonstrated,[2]

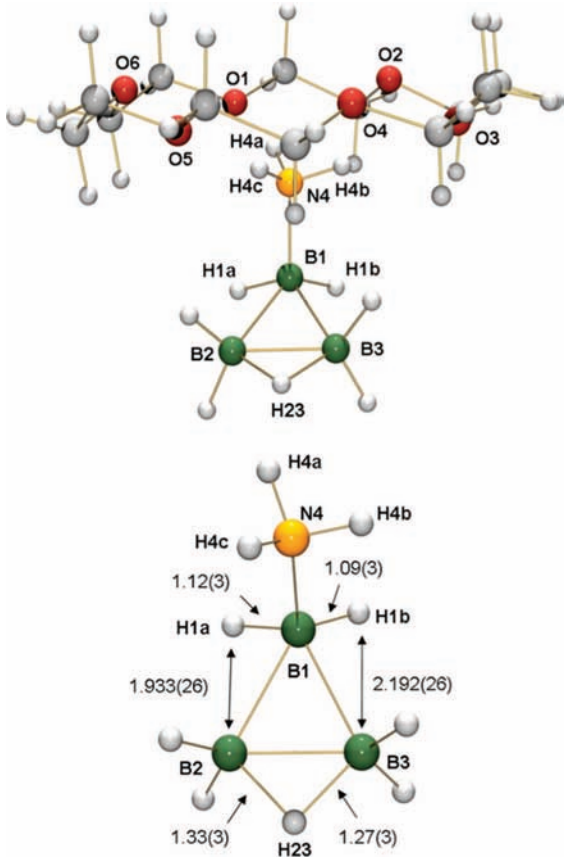

Figure 9. (top) X-ray crystal structure of **1**·18-crown-6 (molecule a) and (bottom) selected distances in the ammonia triborane fragment of **1**·18-crown-6 (molecule a).

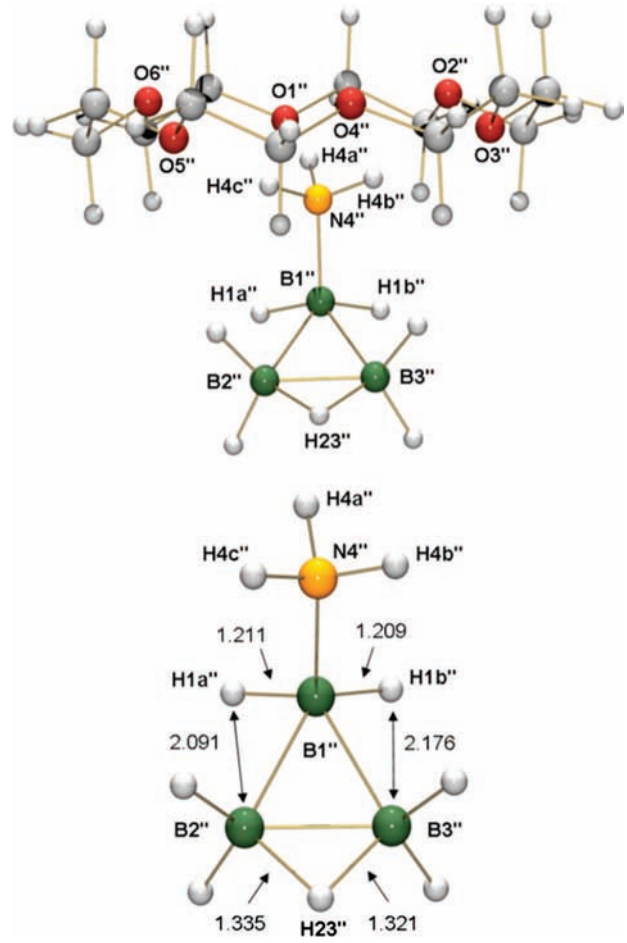

Figure 10. (top) DFT-optimized structure of **1**·18-crown-6 (molecule a); (bottom) selected calculated distances in the ammonia triborane fragment of **1**·18-crown-6 (molecule a).

and as shown by the quantitative gas buret measurements of H_2 release presented in Figure 12a, analogous reactions of 12 mg (0.21 mmol) of **1** with an excess of aqueous HCl (1 mL of 12.1 M HCl) gave a near-theoretical value (eq 9) of 7.85 H_2 equiv (1.65 mmol) over ~1 h.

$$NH_3B_3H_7 + HCl + 6H_2O \rightarrow NH_4^+ + Cl^- + \text{“}3BO_2^-\text{”} + 3H^+\text{”} + 8H_2 \quad (9)$$

The rate of acid hydrolysis was dependent upon the amount of acid used. Thus, when 5.0 equiv of HCl was reacted with a 4.9 wt % solution of **1**, 7.0 H_2 equiv were liberated in 95 min (Figure 12b), whereas a reaction with 3.0 equiv of HCl liberated 5.7 H_2 equiv after 310 min and a reaction with only 1.0 equiv of HCl gave less than 1.0 H_2 equiv after 350 min.

Previous computational studies[5f,17] of the acid-induced dehydrogenation of ammonia borane and ammonia triborane both support a mechanism involving the initial elimination of 1 equiv of H_2 via the reaction of the acid proton with a hydridic B−H hydrogen of the amine boranes. In aqueous solutions, subsequent electrophilic association of the resulting cationic species (i.e., $NH_3BH_2^+$ and $NH_3B_3H_6^+$) with water would then be expected to lead to the observed rapid H_2 release and formation of borates.

More rapid hydrogen release was achieved without acids by using metals to catalyze the hydrolysis reaction (eq 10).

$$NH_3B_3H_7 + 6H_2O \xrightarrow{\text{Metal catalyst}} NH_4^+ + \text{“}3BO_2^- + 2H^+\text{”} + 8H_2(g) \quad (10)$$

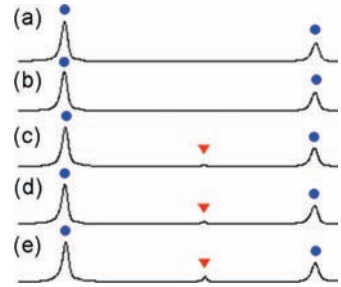

Figure 11. ^{11}B NMR spectra of a 20 wt % aqueous solution of **1** at room temperature after (a) 0 h, (b) 24 h, (c) 96 h, (d) 147 h, (e) 11 days (●, $NH_3B_3H_7$; ▼, NH_3BH_3).

Hydrogen release from $NaBH_4$ and NH_3BH_3 has previously been attained by metal-catalyzed hydrolysis, with Ru catalysts[1a,b] for $NaBH_4$ and Pt catalysts[2e] for NH_3BH_3 exhibiting the highest reactivities. A variety of these and other potential catalysts were screened for activating the hydrolysis of **1**, including Rh(0), Ru(0), Pd(0), and Pt(0) supported on alumina or carbon; $RhCl_3$, $[Rh(COD)Cl]_2$, $RuCl_3$, and $NiCl_2$ metal halides; and nano- or microsized metal or NiB_2 powders. As shown in the examples in Figure 13, catalytic activity was found to be highly dependent upon the particular metal, kind of supports, and degree of dispersed catalytic sites.

(17) Stephens, F. H.; Baker, R. T.; Matus, M. H.; Grant, D. J.; Dixon, D. A. *Angew. Chem., Int. Ed.* **2007**, *46* (5), 746–749.

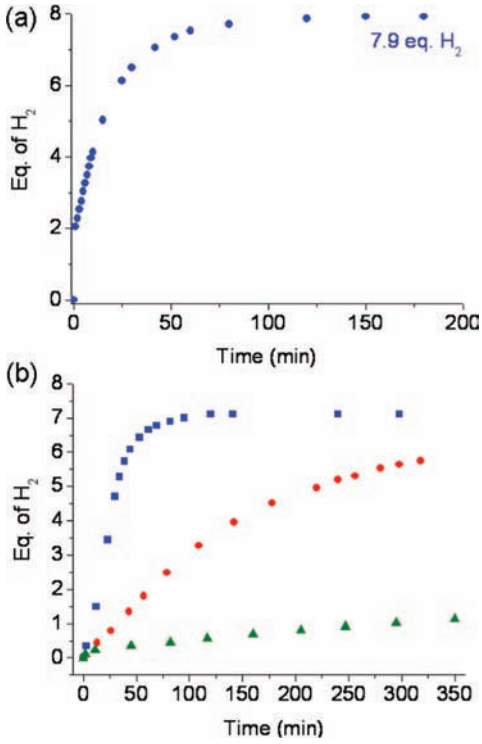

Figure 12. Hydrogen release from (a) a 0.45 wt % aqueous solution of **1** upon reaction with excess HCl and (b) a 4.9 wt % aqueous solution of **1** upon reaction with ■, 5.0; ●, 3.0; or ▲, 1.0 equiv of hydrochloric acid.

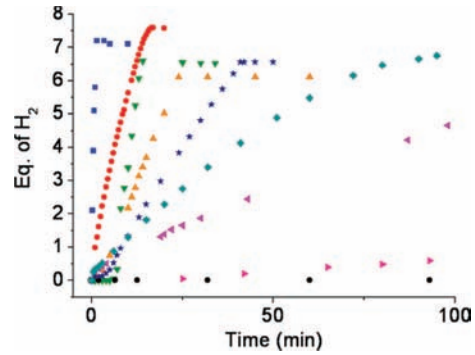

Figure 13. Metal-catalyzed hydrolytic H_2 release from aqueous (0.45 wt %) solution of **1** containing (■) $RhCl_3$ (6.9 mol %); (●) 5 wt % Rh/Al_2O_3 (7.0 mol % Rh); (▼) $RuCl_3$ (7.1 mol %) (inset); (▲) $[Rh(COD)\mu\text{-}Cl]_2$ (7.1 mol %); (star) Ni_xB (35−41 mol %); (◆) 5 wt % Ru supported on ion exchange resins (6.3 mol %); (left-pointing triangle) 5 wt % Pd/Al_2O_3 (6.7 mol %); (right-pointing triangle) Ru powder (22.6 mol %); (•) 5 wt % Rh/C (5.3 mol %), $NiCl_2$ (6.9 mol %), Ni powder (nanosize, 38.6 mol %), Pd powder (sub-micrometer size, 9.0 mol %), Pt powder (nanosize, 6.5 mol %), 5 wt % Ru/Al_2O_3 (7.3 mol %), (For these metal catalysts, the amount of hydrogen was measured up to 120 min.) or no catalyst.

The rhodium-based systems, Rh(0) supported on alumina and $RhCl_3$, proved to be the most active. For example, 5 wt % Rh(0) supported on alumina gave over 7.5 H_2 equiv in 15 min, while $RhCl_3$ yielded ∼7 H_2 equiv in only 1.5 min. Although they were unchanged upon initially dissolving in water, both $[Rh(COD)(\mu\text{-}Cl)]_2$ and $RhCl_3$ appeared to undergo reduction upon addition of **1** suggesting that Rh clusters and/or colloids may be the active catalytic species in these systems.[18] In contrast, neither 5 wt % Rh supported on carbon nor 5 wt % Ru supported on alumina

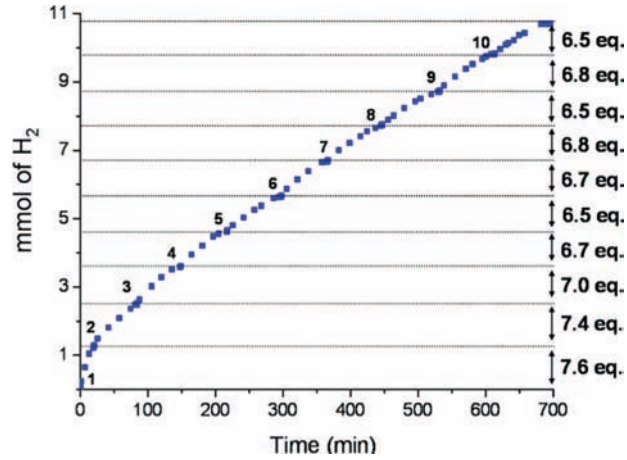

Figure 14. Hydrogen evolution following repeated additions (11 cycles) of **1** to a borate-buffered solution containing 5 wt % Rh/Al_2O_3.

afforded a measurable amount of hydrogen in 2 h. Although 5 wt % Pd/Al_2O_3, Ru(0) supported on an ion-exchange resin and nickel boride also showed significant catalytic activity, their reactivities were much less than either 5 wt % Rh/Al_2O_3 or $RhCl_3$, with less than 7.0 H_2 equiv being evolved in 40 min. Ru powder (22.6 mol%) was much less active, exhibiting less than 3 H_2 equiv in 400 min. Ni, Pd, and Pt powders and $NiCl_2$ showed negligible H_2 release in 2 h.

Unlike the immediate reaction observed with $RhCl_3$, the hydrolysis reaction of **1** with 7.1 mol % of $RuCl_3$ showed an induction period of ∼5−10 min. The formation of black particles during this time suggests reduction of the $RuCl_3$ to form catalytically active Ru(0). A similar induction period was previously observed for $NaBH_4$ catalyzed by Ru supported on carbon (2 wt % Ru).[1d]

The pH of a 0.45 wt % aqueous solution of **1** increased to above 8 after hydrolysis in the presence of $[Rh(COD)Cl]_2$, and if more **1** was then added to this solution, then a decrease in the rate of H_2 release was observed. On the other hand, if a borate buffer was used to maintan the solution pH, then the Rh/Al_2O_3 catalyst exhibited an extended lifetime. As indicated in Figure 14, hydrogen evolution measurements following periodic additions of ∼9 mg (∼0.16 mmol) of solid **1** to a 2 mL aqueous borate-buffered (pH maintained between 7.2 and 8.0) solution containing 1.3 mg (0.012 mmol Rh) of 5 wt % Rh/Al_2O_3 showed little change in the hydrogen release rates over 11 cycles.

The "BO_2^-" product shown in eqs 9 and 10 is only a hypothetical formulation, with the actual borate products of these reactions depending upon the final solution concentration and pH. The ^{11}B NMR spectrum in Figure 15a of a solution obtained after the metal-catalyzed hydrolysis of a 0.45 wt % solution of **1**, exhibits a signal in the 15−17 ppm range resulting from a fast-exchanging equilibrium mixture of $B(OH)_3/B(OH)_4^-$, along with a weak signal at 12.4 ppm from $B_3O_3(OH)_4^-$.[19] With more concentrated solutions of **1** (Figure 15b (4.9 wt %) and c (22.7 wt %)), the signals for the condensed borates $B_3O_3(OH)_4^-$ and $B_5O_6(OH)_4^-$ were dominant.[19] Thus, although the 5 wt % Rh/Al_2O_3 showed extended catalytic activity for the hydrolysis of the diluted solution of **1**, more concentrated solutions will probably not exhibit such extended activity because the borates will precipitate from the solutions and coat the catalyst surface.

(18) (a) Chen, Y.; Fulton, J.; Linehan, J.; Autrey, T. *Prepr. Sym., Div. Fuel Chem.* **2004**, *49*, 972–973. (b) Schulz, J.; Roucoux, A.; Patin, H. *Chem. Commun.* **1999**, 535–536.

(19) (a) Momii, R. K.; Nachtrieb, N. H. *Inorg. Chem.* **1967**, *6*, 1189–1192. (b) Smith, H. D., Jr.; Wiersema, R. J. *Inorg. Chem.* **1972**, *11*, 1152–1154. (c) Salentine, C. G. *Inorg. Chem.* **1983**, *22*, 3920–3924.

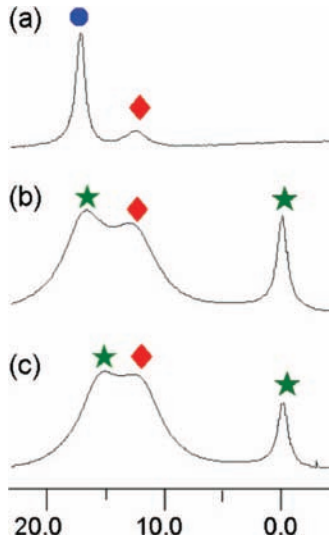

Figure 15. ^{11}B NMR spectra of aqueous **1** solutions (a) after hydrolysis of 0.45 wt %, (b) after hydrolysis of 4.9 wt %, and (c) after hydrolysis of 22.7 wt % aqueous solution; ●, an equilibrium mixture of $B(OH)_3$ and $B(OH)_4^-$; ◆, $B_3O_3(OH)_4^-$; ★, $B_5O_6(OH)_4^-$.

Similar to the results previously observed for the catalyzed $NaBH_4$[1a,c,d] and NH_3BH_3[2i,j] hydrolysis reactions, the H_2-release rate appeared to be independent of the concentration of **1** with, for example, identical rates observed for 4.9 and 22.7 wt % solutions of **1** with 5 wt % Rh/Al_2O_3 (1.1 mol % Rh). However, the H_2-release rates of the 5 wt % Rh/Al_2O_3 and $RhCl_3$ could be effectively controlled and tuned by adjusting the catalyst loadings and reaction temperatures. As illustrated in Figure 16a for 5 wt % Rh/Al_2O_3-catalyzed reactions, while a 1.4 mol % Rh loading gave 5.4 H_2 equiv in 3 h, 7.0 mol % of Rh gave 7.6 H_2 equiv in only 17 min. For a $RhCl_3$-catalyzed reaction, 1.4 mol % Rh gave 5.6 H_2 equiv in 40 min, while 6.9 mol % Rh gave 7.0 H_2 equiv in only 2 min.

As shown in Figure 16b, at 50 °C over 7 H_2 equiv were produced in 25 min from a 4.9 wt % aqueous solution of **1** catalyzed by 5 wt % Rh/Al_2O_3 (1.1 mol % Rh). Decreased rates were observed at lower temperatures, but even at 0 °C, 6 H_2 equiv were released in 17 h. An Arrhenius plot of the H_2-release rate data from a 5 wt % Rh/Al_2O_3 (1.1 mol % Rh) catalyzed reaction of a 4.9 wt % **1** solution at different temperature yielded an activation energy (13.4 kcal/mol) in the range found for metal-catalyzed $NaBH_4$ hydrolysis (~9−18 kcal/mol, depending on the catalyst[1a−f]).

Calculations of the standard heats of hydrolysis from the standard enthalpies of formation, using Dixon's value for the heat of formation of solid $NH_3B_3H_7$ (−24.2 kcal/mol),[5d] indicate that H_2 release from $NH_3B_3H_7$ is slightly more exothermic (18.9 kcal/mol H_2) than from either $NaBH_4$ (14.9 kcal/mol H_2) or NH_3BH_3 (12.7 kcal/mol H_2) but is much less exothermic than the hydrolytic reactions of metal hydrides ($LiAlH_4$ (29.0 kcal/mol H_2), MgH_2 (33.5 kcal/mol H_2), and LiH (31.6 kcal/mol H_2).[20]

The hydrolysis reaction of a highly concentrated 22.7 wt % sample containing 0.30 g of H_2O, 0.10 g of **1** (1.8 mmol) and 0.04 g of 5 wt % Rh/Al_2O_3 (0.02 mmol of Rh) produced 0.027 g (13.5 mmol, 7.5 equiv) of H_2 over 3 h at 21 °C. Since the excess water solvent and catalyst must also be included as a material weight, this mixture corresponds to a 6.1 materials-wt % H_2 [i.e., mat-wt % H_2 = H_2 wt/($NH_3B_3H_7$ + H_2O + Rh/Al_2O_3-wts)]. Therefore, the longer-term DOE total-system H_2-storage targets (2015, 9.0 wt %)[21] for transportation will not be attainable with this, or any other, hydrolytic-based system. Nevertheless, an ammonia triborane-based hydrolytic system can provide a means of safe hydrogen generation that should be competitive with both the NH_3BH_3- and $NaBH_4$-based hydrolysis systems for other applications having less stringent weight requirements. As will be discussed in future publications, the efficient synthesis of **1** that was reported herein is now enabling our ongoing explorations of these and other potential applications, as well as our systematic investigation of the chemistry of this unique compound.

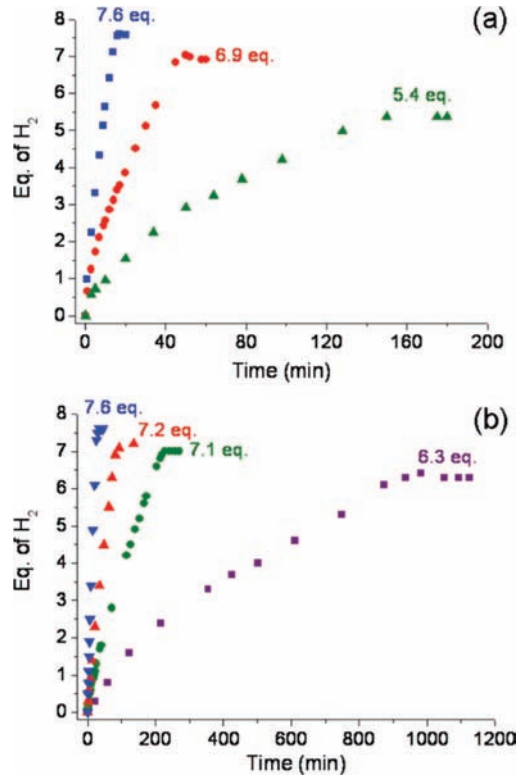

Figure 16. (a) Effect of catalyst loadings on H_2-release rates from a 0.45 wt % aqueous solution of **1** with different amounts of 5 wt % Rh/Al_2O_3 (■, 7.0; ●, 2.9; ▲, 1.4 mol %) and (b) the effect of temperature on H_2 release from a 4.9 wt % aqueous solution of **1** catalyzed by 5 wt % Rh/Al_2O_3 (1.1 mol% Rh). (▼, 50; ▲, 35; ●, 25; ■, 0 °C).

Acknowledgment. We thank the U.S. Department of Energy for grants from the Division of Energy Efficiency and Renewable Energy through the Center of Excellence for Chemical Hydrogen Storage and from the Division of Basic Energy Sciences for the support of this research. We also thank Dr. Goji Kodama for his helpful comments.

Supporting Information Available: Tables of experimental decomposition and hydrolytic H_2-release data for ammonia triborane and tables listing the Cartesian coordinates for all DFT-optimized geometries; complete ref 10a. This material is available free of charge via the Internet at http://pubs.acs.org.

JA808045P

(20) (a) Messer, C. E.; Fasolino, L. G.; Thalmayer, C. E. *J. Am. Chem. Soc.* **1955**, *77*, 4524–4526. (b) Davis, W. D.; Mason, L. S.; Stegeman, G. *J. Am. Chem. Soc.* **1949**, *71*, 2775–2781.

(21) http://www.eere.energy.gov/hydrogenandfuelcells/storage/pdfs/targets_onboard_hydro_storage.pdf.